Mon. Not. R. astr. Soc. (1986) **220,** 801–824

Theoretical studies of interstellar molecular shocks – III. The formation of CH^+ in diffuse clouds

G. Pineau des Forêts *DAPHE, Observatoire de Paris, F-92195 Meudon Principal, France*

D. R. Flower *Physics Department, The University, South Road, Durham DH1 3LE*

T. W. Hartquist *MPI für extraterrestrische Physik, D-8046 Garching bei München, FRG*

A. Dalgarno *Center for Astrophysics, Harvard College Observatory, Cambridge, Massachusetts 02138, USA*

Accepted 1986 January 6. Received 1985 December 23; in original form 1985 October 4

Summary. We present the results of computations of both one-fluid hydrodynamic and three-fluid magnetohydrodynamic models of interstellar molecular shocks. A network of over 150 chemical reactions was incorporated in the models with a view to correctly predicting the variation of the fractional ionization in the precursors of MHD shocks and the column densities of a number of chemical species, particularly CH^+, which may be selectively formed in shocks. We find that one-fluid hydrodynamic models predict column densities of CH^+ which are too small to be considered compatible with observations. The MHD models are more successful in this respect, CH^+ being formed by the endothermic $C^+(H_2,H)CH^+$ reaction, driven by ambipolar diffusion. However, difficulties remain in simultaneously reproducing the observed column densities of other species which are formed in shocks, specifically the excited rotational states of H_2.

1 Introduction

The problem of the formation of CH^+ in the diffuse interstellar medium has a long history, reviewed to 1975 by Dalgarno (1976). It has since been suggested that CH^+ may form preferentially in shocks (Elitzur & Watson 1978, 1980), the endothermic reaction

$$C^+ + H_2 \rightarrow CH^+ + H - 4640\,K \qquad (1.1)$$

being driven by the thermal energy of the post-shock gas. This suggestion was based on the results of calculations for one-fluid, hydrodynamic shocks, with a network of 20 chemical reactions. A much more complete chemical scheme has since been included in such models by Mitchell & Deveau (1983).

In addition to CH^+, a number of other species may be produced in shocks, including OH through the reaction

$$O + H_2 \rightarrow OH + H - 2980\,K, \tag{1.2}$$

and excited rotational states of H_2. A satisfactory model of shock formation should be able to simultaneously reproduce the observed column densities of all these species.

Since the work of Mullan (1971), it has been known that the presence of even a weak magnetic field, perpendicular to the direction of motion of the shock, may greatly perturb the shock structure. Substantial differences can develop between the flow speeds and kinetic temperatures of ionized and neutral species. As a consequence, the maximum temperature within the shock is substantially reduced, as compared with the value behind a hydrodynamic shock with the same speed, and the width of the 'warm' region is considerably enhanced (Draine 1980). For these reasons alone, it might be anticipated that the chemistry induced in magnetohydrodynamic (MHD) shocks should differ appreciably from expectations based on models of one-fluid, hydrodynamic shocks. In particular, ion–neutral streaming (ambipolar diffusion) might drive important ion–molecule reactions, such as (1.1) above.

Not only does the structure of the shock affect the chemistry, but the chemistry significantly affects the structure of a MHD shock. Ion–molecule reactions such as (1.1) are followed by dissociative recombination, leading to the removal of an important fraction of the ionized component of the gas. The maximum temperature attained within the shock is further reduced and the width of the shock increased [Flower, Pineau des Forêts & Hartquist 1985 (Paper I)]. Thus, in order to correctly determine the structure of the shock, careful attention must be paid to reactions which alter the degree of ionization of the gas.

In Section 2, we describe the chemical network (approximately 150 reactions) included in the present study. Section 3 summarizes the results which have been obtained for grids of both hydrodynamic and MHD models. The abundances of important chemical species are plotted as functions of distance through the shock for a representative MHD model.

The results are discussed in relation to the observed column densities of species, particularly CH^+, which may be formed in shocks. Our conclusions are given in Section 4.

2 The chemical model

The importance of the ion–neutral chemistry for the evolution of the ionization structure in a shock in a diffuse cloud was demonstrated in Paper I. The ionization structure determines the efficiency of ion–neutral coupling and, hence, the magnetic and flow structures, the dissipation rate and the thermal structure. The shock structure in turn affects many of the rates at which neutral–neutral and ion–molecule reactions occur. Any quantitative theoretical study of the chemistry in MHD shocks in diffuse molecular clouds must include the dominant reactions leading to the creation and removal of the most abundant ions. In quiescent diffuse clouds the most abundant ions are C^+ and H^+. We also include He^+, which has a nearly constant flux through the shock. In extreme cases, when C^+, H^+ and the molecular ions formed from them are almost removed, He^+ could dominate the ion mass. The photo-ionization of neutral atomic carbon (reaction 87 in Table 1) maintains the upstream C^+ abundance and the cosmic rays ionize H, H_2, and He (reactions 83–86).

2.1 CHEMISTRY IN A MOLECULAR MEDIUM IN WHICH PHOTO-REACTIONS ARE SLOW

Initially, we restrict our attention to diffuse molecular regions in which the abundance ratio of H_2 to H is large and the UV radiation field is strong enough to ensure that C^+ is abundant

Table 1. The chemical reaction network. Rate coefficients for photoprocesses (and cosmic ray ionization) are represented as $k=\gamma s^{-1}$ ($\zeta=4\times10^{-17}s^{-1}$). The rate coefficients for the remaining reactions are listed as $k=\gamma(T/300)^{\alpha}\exp(-\beta/T)\,cm^3s^{-1}$ where T is the temperature in Kelvin. Numbers in brackets are powers of 10.

	Reaction	α	β	γ	References and notes
1	$C^+ + H_2 \rightarrow CH^+ + H$	0.0	4640	1.0 (-10)	1, 2, 3, 4, *a*
2	$CH^+ + H_2 \rightarrow CH_2^+ + H$	0.0	0.0	1.2 (- 9)	5
3	$CH_2^+ + H_2 \rightarrow CH_3^+ + H$	0.0	0.0	7.0 (-10)	6
4	$CH_3^+ + H_2 \rightarrow CH_4^+ + H$	0.0	32500	2.0 (-10)	6, b
5	$CH_3^+ + H_2 \rightarrow CH_5^+ + h\nu$	-1.0	0.0	3.3 (-15)	7, c
6	$CH_4^+ + H_2 \rightarrow CH_5^+ + H$	0.0	0.0	4.0 (-11)	6
7	$CH^+ + H \rightarrow C^+ + H_2$	0.0	0.0	1.0 (-10)	1, 2, 3, *a*
8	$CH_2^+ + H \rightarrow CH^+ + H_2$	0.0	400	1.2 (- 9)	5
9	$CH_3^+ + H \rightarrow CH_2^+ + H_2$	0.0	10560	7.0 (-10)	6
10	$CH_4^+ + H \rightarrow CH_3^+ + H_2$	0.0	0.0	2.0 (-10)	6
11	$CH_5^+ + H \rightarrow CH_4^+ + H_2$	0.0	4000	4.0 (-11)	6, b
12	$C + H_2 \rightarrow CH + H$	0.5	14100	1.2 (- 9)	8
13	$CH + H_2 \rightarrow CH_2 + H$	0.67	8820	2.3 (-11)	8
14	$CH_2 + H_2 \rightarrow CH_3 + H$	0.17	6400	5.2 (-11)	8
15	$CH_3 + H_2 \rightarrow CH_4 + H$	0.0	5460	3.0 (-10)	9
16	$CH + H \rightarrow C + H_2$	0.5	2200	1.2 (- 9)	8
17	$CH_2 + H \rightarrow CH + H_2$	0.67	12850	2.3 (-11)	8
18	$CH_3 + H \rightarrow CH_2 + H_2$	0.17	5600	5.2 (-11)	8
19	$CH_4 + H \rightarrow CH_3 + H_2$	0.0	6560	3.0 (-10)	9, c
20	$C^+ + e \rightarrow C + h\nu$	-0.61	0.0	4.4 (-12)	10
21	$CH^+ + e \rightarrow C + H$	-0.5	0.0	2.9 (- 7)	11
22	$CH_2^+ + e \rightarrow C + H_2$	-0.5	0.0	2.5 (- 7)	11
23	$CH_2^+ + e \rightarrow CH + H$	-0.5	0.0	2.5 (- 7)	11
24	$CH_3^+ + e \rightarrow CH_2 + H$	-0.5	0.0	1.7 (- 7)	11
25	$CH_3^+ + e \rightarrow CH + H_2$	-0.5	0.0	3.5 (- 7)	11
26	$CH_3^+ + e \rightarrow CH + H + H$	-0.5	0.0	1.7 (- 7)	11
27	$CH_4^+ + e \rightarrow CH_3 + H$	-0.5	0.0	3.7 (- 7)	11
28	$CH_4^+ + e \rightarrow CH_2 + H_2$	-0.5	0.0	3.7 (- 7)	11
29	$CH_5^+ + e \rightarrow CH_3 + H_2$	-0.5	0.0	5.4 (- 7)	12
30	$CH_5^+ + e \rightarrow CH_4 + H$	-0.5	0.0	5.4 (- 7)	12
31	$O + H_2 \rightarrow OH + H$	2.8	2980	1.5 (-13)	13
32	$OH + H_2 \rightarrow H_2O + H$	2.0	1490	9.5 (-13)	13

Table 1 – *continued*

	Reaction	α	β	γ	References and notes
33	$OH + H \rightarrow O + H_2$	2.8	1950	7.0 (-14)	13
34	$H_2O + H \rightarrow OH + H_2$	1.9	9265	5.2 (-12)	13
35	$H^+ + H_2 \rightarrow H_2^+ + H$	0.0	21300	1.0 (-10)	10
36	$H_2^+ + H \rightarrow H^+ + H_2$	0.0	0.0	1.0 (-10)	10
37	$H_3^+ + H \rightarrow H_2^+ + H_2$	0.0	20000	2.1 (- 9)	10
38	$H_2^+ + H_2 \rightarrow H_3^+ + H$	0.0	0.0	2.1 (- 9)	10
39	$H^+ + O \rightarrow O^+ + H$	0.0	227	1.0 (- 9)	14
40	$H^+ + OH \rightarrow OH^+ + H$	0.0	0.0	2.1 (- 9)	10
41	$H^+ + H_2O \rightarrow H_2O^+ + H$	0.0	0.0	8.2 (- 9)	10
42	$H^+ + CH \rightarrow CH^+ + H$	0.0	0.0	1.9 (- 9)	10
43	$H^+ + CH_2 \rightarrow CH^+ + H_2$	0.0	0.0	1.4 (- 9)	10
44	$H^+ + CH_2 \rightarrow CH_2^+ + H$	0.0	0.0	1.4 (- 9)	10
45	$H^+ + CH_3 \rightarrow CH_3^+ + H$	0.0	0.0	3.4 (- 9)	10
46	$H^+ + CH_4 \rightarrow CH_3^+ + H_2$	0.0	0.0	2.3 (- 9)	10
47	$H^+ + CH_4 \rightarrow CH_4^+ + H$	0.0	0.0	1.5 (- 9)	10
48	$H_2^+ + C \rightarrow CH^+ + H$	0.0	0.0	2.4 (- 9)	10
49	$H_2^+ + O \rightarrow OH^+ + H$	0.0	0.0	1.5 (- 9)	10
50	$H_2^+ + OH \rightarrow OH^+ + H_2$	0.0	0.0	7.6 (-10)	10
51	$H_2^+ + H_2O \rightarrow H_2O^+ + H_2$	0.0	0.0	3.9 (- 9)	10
52	$H_2^+ + H_2O \rightarrow H_3O^+ + H$	0.0	0.0	3.4 (- 9)	10
53	$H_2^+ + CH \rightarrow CH^+ + H_2$	0.0	0.0	7.1 (-10)	10
54	$H_2^+ + CH \rightarrow CH_2^+ + H$	0.0	0.0	7.1 (-10)	10
55	$H_2^+ + CH_2 \rightarrow CH_3^+ + H$	0.0	0.0	1.0 (- 9)	10
56	$H_2^+ + CH_2 \rightarrow CH_2^+ + H_2$	0.0	0.0	1.0 (- 9)	10
57	$H_2^+ + CH_3 \rightarrow CH_3^+ + H_2$	0.0	0.0	1.0 (- 9)	15
58	$H_2^+ + CH_4 \rightarrow CH_4^+ + H_2$	0.0	0.0	1.4 (- 9)	10
59	$H_2^+ + CH_4 \rightarrow CH_5^+ + H$	0.0	0.0	1.1 (-10)	10
60	$H_2^+ + CH_4 \rightarrow CH_3^+ + H_2 + H$	0.0	0.0	2.3 (- 9)	10
61	$H_3^+ + C \rightarrow CH^+ + H_2$	0.0	0.0	2.0 (- 9)	10
62	$H_3^+ + O \rightarrow OH^+ + H_2$	0.0	0.0	8.0 (-10)	10
63	$H_3^+ + OH \rightarrow H_2O + H_2$	0.0	0.0	1.3 (- 9)	10
64	$H_3^+ + H_2O \rightarrow H_3O^+ + H_2$	0.0	0.0	5.9 (- 9)	10
65	$H_3^+ + CH \rightarrow CH_2^+ + H_2$	0.0	0.0	1.2 (- 9)	10
66	$H_3^+ + CH_2 \rightarrow CH_3^+ + H_2$	0.0	0.0	1.7 (- 9)	10

Table 1 – *continued*

	Reaction	α	β	γ	References and notes
67	$H_3^+ + CH_3 \rightarrow CH_4^+ + H_2$	0.0	0.0	2.1 (- 9)	10
68	$H_3^+ + CH_4 \rightarrow CH_5^+ + H_2$	0.0	0.0	2.4 (- 9)	10
69	$He^+ + H_2 \rightarrow H^+ + H + He$	0.0	0.0	1.5 (-13)	10
70	$He^+ + OH \rightarrow O^+ + H + He$	0.0	0.0	1.1 (- 9)	10
71	$He^+ + H_2O \rightarrow H_2O^+ + He$	0.0	0.0	7.0 (-11)	10
72	$He^+ + H_2O \rightarrow OH^+ + H + He$	0.0	0.0	3.7 (-10)	10
73	$He^+ + CH \rightarrow C^+ + H + He$	0.0	0.0	1.1 (- 9)	10
74	$He^+ + CH_2 \rightarrow CH^+ + H + He$	0.0	0.0	4.9 (-10)	10
75	$He^+ + CH_3 \rightarrow CH^+ + H_2 + He$	0.0	0.0	1.8 (- 9)	10
76	$He^+ + CH_4 \rightarrow CH_2^+ + H_2 + He$	0.0	0.0	9.3 (-10)	10
77	$He^+ + CH_4 \rightarrow CH_3^+ + H + He$	0.0	0.0	6.3 (-11)	10
78	$He^+ + CH_4 \rightarrow CH_4^+ + He$	0.0	0.0	3.8 (-11)	10
79	$H^+ + e \rightarrow H + h\nu$	-0.75	0.0	3.6 (-12)	10
80	$H_2^+ + e \rightarrow H + H$	-0.50	0.0	9.8 (- 9)	16
81	$H_3^+ + e \rightarrow H_2 + H$	-0.50	0.0	9.8 (- 9)	12
82	$He^+ + e \rightarrow He + h\nu$	-0.67	0.0	4.5 (-12)	10
83	$CR + H \rightarrow H^+ + e$	0.0	0.0	0.46 ζ	10, e
84	$CR + H_2 \rightarrow H^+ + H + e$	0.0	0.0	0.022 ζ	10, e
85	$CR + H_2 \rightarrow H_2^+ + e$	0.0	0.0	0.93 ζ	10, e
86	$CR + He \rightarrow He^+ + e$	0.0	0.0	0.50 ζ	10, e
87	$C + h\nu \rightarrow C^+ + e$	0.0	0.0	1.6 (-10)	17
88	$CH + h\nu \rightarrow C + H$	0.0	0.0	2.5 (-10)	17
89	$CH + h\nu \rightarrow CH^+ + e$	0.0	0.0	3.0 (-10)	17
90	$CH_2 + h\nu \rightarrow CH + H$	0.0	0.0	5.0 (-11)	15
91	$CH_2 + h\nu \rightarrow CH_2^+ + e$	0.0	0.0	3.0 (-10)	20
92	$CH_3 + h\nu \rightarrow CH + H_2$	0.0	0.0	3.0 (-11)	20
93	$CH_3 + h\nu \rightarrow CH_2 + H$	0.0	0.0	3.0 (-11)	20
94	$CH_3 + h\nu \rightarrow CH_3^+ + e$	0.0	0.0	1.0 (-10)	20
95	$CH_4 + h\nu \rightarrow CH_3 + H$	0.0	0.0	2.1 (-10)	17
96	$CH_4 + h\nu \rightarrow CH_2 + H_2$	0.0	0.0	6.2 (-10)	17
97	$CH_4 + h\nu \rightarrow CH + H_2 + H$	0.0	0.0	2.1 (-10)	17
98	$CH_4 + h\nu \rightarrow CH_4^+ + e$	0.0	0.0	3.0 (-10)	18
99	$OH + h\nu \rightarrow O + H$	0.0	0.0	4.0 (-10)	19
100	$H_2O + h\nu \rightarrow H_2O^+ + e$	0.0	0.0	1.0 (-11)	17

Table 1 – *continued*

	Reaction	α	β	γ	References and notes
101	$H_2O + h\nu \rightarrow OH + H$	0.0	0.0	5.6 (-10)	17
102	$H_2O + h\nu \rightarrow O + H_2$	0.0	0.0	5.6 (-11)	17
103	$H_2^+ + h\nu \rightarrow H^+ + H$	0.0	0.0	2.6 (-10)	20
104	$H_3^+ + h\nu \rightarrow H_2^+ + H$	0.0	0.0	5.0 (-12)	15
105	$H_3^+ + h\nu \rightarrow H^+ + H_2$	0.0	0.0	1.0 (-11)	15
106	$CH^+ + h\nu \rightarrow H^+ + C$	0.0	0.0	2.0 (-10)	17
107	$CH_2^+ + h\nu \rightarrow CH^+ + H$	0.0	0.0	1.7 (- 9)	20
108	$CH_3^+ + h\nu \rightarrow CH^+ + H_2$	0.0	0.0	1.0 (- 9)	20
109	$CH_3^+ + h\nu \rightarrow CH_2^+ + H$	0.0	0.0	1.0 (- 9)	20
110	$CH_4^+ + h\nu \rightarrow CH_3^+ + H$	0.0	0.0	1.0 (- 9)	15
111	$CH_4^+ + h\nu \rightarrow CH_2^+ + H_2$	0.0	0.0	1.0 (- 9)	15
112	$CH_5^+ + h\nu \rightarrow CH_3^+ + H_2$	0.0	0.0	1.0 (- 9)	15
113	$CH_5^+ + h\nu \rightarrow CH_4^+ + H$	0.0	0.0	1.0 (- 9)	15
114	$O^+ + H \rightarrow H^+ + O$	0.0	0.0	1.0 (- 9)	14
115	$O^+ + H_2 \rightarrow OH^+ + H$	0.0	0.0	1.6 (- 9)	10
116	$OH^+ + H_2 \rightarrow H_2O^+ + H$	0.0	0.0	1.1 (- 9)	10
117	$H_2O^+ + H_2 \rightarrow H_3O^+ + H$	0.0	0.0	6.1 (-10)	10
118	$OH^+ + H \rightarrow O^+ + H_2$	0.0	7500	1.6 (- 9)	10
119	$H_2O^+ + H \rightarrow OH^+ + H_2$	0.0	11000	1.1 (- 9)	10
120	$H_3O^+ + H \rightarrow H_2O^+ + H_2$	0.0	20500	6.1 (-10)	10
121	$O^+ + e \rightarrow O + h\nu$	-0.63	0.0	3.4 (-12)	10
122	$OH^+ + e \rightarrow O + H$	-0.50	0.0	7.5 (- 8)	21
123	$H_2O^+ + e \rightarrow OH + H$	-0.50	0.0	3.9 (- 7)	21
124	$H_2O^+ + e \rightarrow O + H_2$	-0.50	0.0	3.9 (- 7)	21
125	$H_3O^+ + e \rightarrow H_2O + H$	-0.50	0.0	6.3 (- 8)	21
126	$H_3O^+ + e \rightarrow OH + H_2$	-0.50	0.0	5.7 (- 7)	21
127	$OH^+ + h\nu \rightarrow H^+ + O$	0.0	0.0	7.2 (-12)	20
128	$OH^+ + h\nu \rightarrow O^+ + H$	0.0	0.0	7.2 (-12)	15
129	$H_2O^+ + h\nu \rightarrow OH^+ + H$	0.0	0.0	3.0 (-10)	15
130	$H_2O^+ + h\nu \rightarrow O^+ + H_2$	0.0	0.0	1.0 (-10)	15
131	$H_2O^+ + h\nu \rightarrow H^+ + OH$	0.0	0.0	1.0 (-10)	15
132	$H_2O^+ + h\nu \rightarrow H_2^+ + O$	0.0	0.0	1.0 (-10)	15
133	$H_3O^+ + h\nu \rightarrow H_2O^+ + H$	0.0	0.0	1.5 (-11)	15
134	$H_3O^+ + h\nu \rightarrow OH^+ + H_2$	0.0	0.0	5.0 (-11)	15
135	$H_3O^+ + h\nu \rightarrow H_2^+ + OH$	0.0	0.0	5.0 (-11)	15
136	$H_3O^+ + h\nu \rightarrow H^+ + H_2O$	0.0	0.0	5.0 (-11)	15
137	$C^+ + OH \rightarrow CO^+ + H$	0.0	0.0	7.7 (-10)	10
138	$C^+ + OH \rightarrow H^+ + CO$	0.0	0.0	7.7 (-10)	15
139	$C^+ + H_2O \rightarrow HCO^+ + H$	0.0	0.0	2.7 (- 9)	10
140	$CH^+ + O \rightarrow CO^+ + H$	0.0	0.0	7.6 (-10)	10

Table 1 – *continued*

	Reaction	α	β	γ	References and notes
141	$CH^+ + OH \rightarrow CO^+ + H_2$	0.0	0.0	7.5 (-10)	10
142	$CH^+ + H_2O \rightarrow HCO^+ + H_2$	0.0	0.0	1.0 (- 9)	10
143	$CH_2^+ + O \rightarrow HCO^+ + H$	0.0	0.0	7.5 (-10)	10
144	$CH_2^+ + OH \rightarrow HCO^+ + H_2$	0.0	0.0	7.4 (-10)	10, f
145	$CH_2^+ + H_2O \rightarrow HCO^+ + H_2 + H$	0.0	0.0	5.2 (-10)	10, g
146	$CH_3^+ + O \rightarrow HCO^+ + H_2$	0.0	0.0	4.4 (-10)	10
147	$CH_3^+ + OH \rightarrow HCO^+ + H_2 + H$	0.0	0.0	7.2 (-10)	10, h
148	$CH_3^+ + H_2O \rightarrow H_3O^+ + CH_2$	0.0	15100	1.0 (- 9)	15
149	$CH_4^+ + H_2O \rightarrow H_3O^+ + CH_3$	0.0	0.0	9.6 (-10)	10
150	$CH_5^+ + OH \rightarrow H_2O^+ + CH_4$	0.0	0.0	7.0 (-10)	10
151	$CH_5^+ + H_2O \rightarrow H_3O^+ + CH_4$	0.0	0.0	9.5 (-10)	10
152	$CO^+ + H_2 \rightarrow HCO^+ + H$	0.0	0.0	2.0 (- 9)	10
153	$HCO^+ + H \rightarrow CO^+ + H_2$	0.0	24500	2.0 (- 9)	10
154	$CO + h\nu \rightarrow C + O$	0.0	0.0	3.0 (-11)	22
155	$CO^+ + h\nu \rightarrow C^+ + O$	0.0	0.0	3.0 (-11)	15
156	$HCO^+ + h\nu \rightarrow CO^+ + H$	0.0	0.0	3.0 (-10)	15
157	$CO^+ + e \rightarrow C + O$	-0.50	0.0	1.8 (- 7)	10
158	$HCO^+ + e \rightarrow CO + H$	-0.50	0.0	1.1 (- 7)	12

References:

(1) Chesnavich, Akin & Webb (1984)
(2) Ervin & Armentrout (1984)
(3) Federer *et al.* (1984)
(4) Adams, Smith & Millar (1984)
(5) Smith & Adams (1977)
(6) Kim, Theard & Huntress (1975)
(7) Herbst (1985)
(8) Aannestad (1973)
(9) Yung & Allen (1983)
(10) Prasad & Huntress (1980)
(11) Mul *et al.* (1981)
(12) Smith & Adams (1984)
(13) Cohen & Westburg (1983)
(14) Chambaud *et al.* (1980)
(15) Estimate
(16) Giusti-Suzor, Bardsley & Derkits (1983)
(17) Roberge *et al.* (1981)
(18) Dalgarno (1952)
(19) van Dischoeck & Dalgarno (1984)
(20) Black & Dalgarno (1977)
(21) Mitchell & McGowan (1983)
(22) Dalgarno (1986)

Notes:

(a) See the discussion in Flower *et al.* (1985).
(b) Note that the heat of formation of CH_4^+ is uncertain and 4000 K is an upper bound to the numerator in the exponential in the rate for reaction 11.
(c) Herbst gave results for various populations of rotational levels in the target molecules. We have used a coefficient with a value between those for the two cases considered by Herbst.
(d) The rate differs from the one used by Mitchell (1984) and was obtained from the rate for reaction 15.
(e) We set $\zeta = 4\times10^{-17}\,s^{-1}$ in all of the models.
(f) The Prasad & Huntress (1980) rate coefficient for the $H_2CO^+ + H$ reaction is adopted. We have simplified the model by assuming that H_2CO^+ is photodissociated rapidly to HCO^+.
(g) The Prasad & Huntress (1980) rate coefficient for the $H_3CO^+ + H$ reaction is adopted. We have simplified the model by assuming that H_3CO^+ is photodissociated rapidly to HCO^+.
(h) The Prasad & Huntress (1980) rate coefficient for the $H_2CO^+ + H_2$ reaction is adopted. We have simplified the model by assuming that H_2CO^+ is photodissociated rapidly to HCO^+.

in the upstream material, but weak enough for photodissociation and photoionization reactions to be slow compared to other reactions in the hot shocked gas. The removal of C^+ in a shock occurs by reaction 1 in the table, $C^+(H_2, H)CH^+$, whenever the temperature or the ion–neutral streaming speed is high. Ions of the type CH_n^+ can react with H_2 (reactions 2–6) to form heavier molecular ions CH_{n+1}^+ or, when radiative association occurs, CH_{n+2}^+. Unless the streaming speed or the temperature becomes unusually high the reaction of CH_3^+ with H_2 is very slow and CH_3^+ becomes the most abundant carbon-bearing ion. Initially, CH_3^+ is removed predominantly by dissociative recombination and the rates of reactions (24–26) are important for determining the initial drop of ionization in the shock. When the fractional ionization has dropped to about 10^{-5}, CH_3^+ is removed primarily by reaction (146) with O. The recombination of H_3O^+ (reactions 125 and 126) is then important in further neutralization of species formed by the sequence initiated by reaction (1). Because of the rapidity of the reaction (41) of H^+ with H_2O to form H_2O^+ which reacts with H_2, the recombination of H_3O^+ is also important as the last step in the neutralization of H^+. One expects at least two neutralization length-scales to be important for the ionization structure of MHD shock in diffuse molecular clouds. They are (i) the length-scale over which the sequence beginning with the $C^+(H_2, H)CH^+$ reaction and ending with the dissociative recombination of CH_3^+ reduces the ionization, and (ii) the length-scale over which CH_3^+ (if no source of ionization maintains the fractional ionization above about 10^{-5}) and H^+ are neutralized in sequences initiated by their reactions with H_2O. The latter length-scale is the larger and, if the fractional concentration of H^+ is above about 3×10^{-5} in the ambient gas, H^+ can become the most abundant ion in some parts of the precursor.

As seen by inspection of reactions (69–78) and (82), the removal of He^+ is dominated by its reaction (69) with H_2. As the formation rate of He^+ (reaction 86) also scales with the neutral density, the upstream and far downstream densities of He^+ are equal; however, the time-scales for He^+ creation and removal are sufficiently long that its flux through the precursor is constant and the He^+ fractional contribution to the mass of the ion fluid increases as other ions are removed.

2.2 CHEMISTRY IN THE PRESENCE OF PHOTOREACTIONS

We now consider the role of photoionization in determining a third important length-scale. If that length-scale is short compared to the two length-scales associated with the neutralization of C^+ and H^+, the ion flux will not drop in the precursor. However, we find in Section 3 that the photoionization length-scale is long enough for a substantial reduction of the ion flux to occur. Photodissociation reactions break down OH_3^+, CH_3^+, and H_2O and the products, CH_2 and CH, of the dissociative recombination of CH_3^+ to smaller species. Reactions (127–136) and reactions (106–113) are the photodissociation reactions for OH_n^+ and for CH_n^+. Reactions (99–102) and reactions (87–98) are the photodissociation and photoionization reactions for OH_n and for C and CH_n.

Though cosmic ray ionization of H_2 (reactions 84 and 85) favours the production of H_2^+ which reacts (reaction 38) with H_2 to form H_3^+, photodissociation of H_3^+ (reactions 104 and 105) and of H_2^+ (reaction 103) leads to the formation of H^+. At high temperature or high streaming speed H^+ can react (reaction 35) with H_2 to form H_2^+, and so H^+, H_2^+, and H_3^+ are all present in the ambient gas, where recombination (reactions 79–81) with electrons is important. Rapid reactions with oxygen-bearing species (e.g. reactions 41, 51, 52 and 64 with H_2O) are also important for their removal.

When photodissociation is included, CH_3^+ is not necessarily the dominant carbon-bearing molecular ion and H_2O is not necessarily the dominant oxygen-bearing neutral. Hence, all

reactions (137–151) of C^+ and CH_n^+ with O and OH_n have been included. For similar reasons all reactions (reactions 39–41, 49–52, 62–64) of H^+ and H_n^+ with O and with OH_n were incorporated in the model. For completeness, all reactions (42–48, 53–60, 61 and 65–68) of H^+ and H_n^+ with C and with CH_n were included. Following the formation of H_3O^+ by, for instance, reaction (148), photodissociation produces O^+, OH^+, and OH_2^+; reactions (115–117) with H_2 then lead to the reformation of H_3O^+. Reactions (12–15) of C and CH_n with H_2 will also convert photodissociation products back into larger molecules. Clearly, the inclusion of photodissociation greatly increases the complexity of the chemistry. In particular C^+, H^+, CH_3^+, and OH_3^+ are not the only important species in determining the ionization structure when photodissociation occurs. As a result all recombination processes (reactions 20–30, 79–81, and 121–126) for C^+, CH_n^+, O^+, OH_n^+, H^+ and H_n^+ must be included.

Elitzur & Watson (1978, 1980) performed calculations for various abundance ratios of H and H_2 in the pre-shock gas. If the density of H is not negligible, reactions of CH_n^+ (reactions 7–11), of CH_n (reactions 16–19), of OH_n (reactions 33 and 34), of H_n^+ (reactions 36 and 37) and of OH_n^+ (reactions 118–120) lead to the removal of one hydrogen atom from the heavy collision partner. In the presence of atomic hydrogen, O^+ is removed by the charge transfer reaction (114). Except for the additions of these reactions, the presence of H does not complicate the model further than the inclusion of photodissociation.

As reactions of C^+ and CH_n^+ with O and OH_n are included, molecular ions and neutrals containing two heavy atoms can be formed. Such products of these reactions are CO, CO^+, and H_nCO^+. Reactions (152–158) are included to complete the description of the chemistry of those species. For simplicity, we have assumed that H_2CO^+ and H_3CO^+ are photodissociated rapidly to form HCO^+. In fact, they are probably progenitors of HCO and H_2CO. This assumption gives rise to similar production rates for CO as the assumption that HCO and H_2CO form rapidly from H_2CO^+ and H_3CO^+ and are quickly photodissociated to form CO. These two assumptions result in different abundances of HCO^+ but give the same value for the CO abundance. The assumption that HCO and H_2CO are formed and photodissociated rapidly is consistent with the results of the reference model, discussed in the next section.

We have not included reactions such as those of C^+ and CH_n^+ with C and CH_n. This specific set of reactions leads to the formation of C_2 and more complex carbon-bearing species. For the purposes of studying the structure of MHD shocks in diffuse molecular clouds, we can model the chemistry of species containing more than one heavy atom in the simple way adopted here. However, HCO, H_2CO, and C_2 are likely to be important signatures of the existence of precursors in diffuse cloud shocks. Precursors provide larger regions in which trace molecules and molecular ions can interreact than are present in one-fluid, hydrodynamic shocks, where discontinuous changes occur in both the ion and neutral flow variables. The chemical model that we have used to calculate the ionization structure can also be employed to study the abundance of CH^+ in MHD shocks.

We note that uncertainties exist in a number of chemical reaction rates. The photoionization and the dissociative recombination rates are of particular importance for the calculation of the ionization structure. Except for the photochemical data from Roberge, Dalgarno & Flannery (1981) and van Dishoeck & Dalgarno (1984), most photochemical rates are no better than educated guesses. For the reference model discussed in the next section, these uncertainties are not too crucial, as atomic carbon and atomic oxygen, for which the photoionization cross-sections are known, are the most abundant heavy neutral species. The results of the reference model also show that C^+ and H^+ are the most abundant ions throughout the precursor. In this case, the key parameters are not the dissociative recombination rates but rather the rates of reaction (1) and of reaction (39), which initiate the sequences leading to molecular-ion formation.

The references for the reaction rate data are given in Table 1. Thermodynamic data for the

ions can be found in the compilations by Rosenstock *et al.* (1977) and by Lias, Liebman & Levin (1984).

Other aspects of the theoretical model are described in Papers I and II. A few modifications have since been made.

(i) In Paper I, we used the concept of an effective temperature for reactions involving an ion and a neutral. This temperature was defined as

$$T_{\rm eff} = T_r + T_s \tag{2.1}$$

where

$$T_r = \frac{m_{\rm i} T_{\rm n} + m_{\rm n} T_{\rm i}}{m_{\rm i} + m_{\rm n}} \tag{2.2}$$

is an ion–neutral kinetic temperature, weighted by the particle masses, and

$$\tfrac{3}{2}\varkappa T_s = \tfrac{1}{2} m_{\rm in} (u_{\rm i} - u_{\rm n})^2 \tag{2.3}$$

is the contribution of the relative macroscopic kinetic energy of the ionized and neutral particles. Expression (2.1) for $T_{\rm eff}$ leads to the rate of the corresponding reaction being overestimated when $T_r < T_s \approx \beta$, where β is the reaction threshold. In order to circumvent this problem, we have taken the ion–molecule reaction rates to be proportional to $\exp\{-\max[\beta/T_{\rm eff}, (\beta - 3T_s)/T_r]\}$. In this way, if T_s approaches β whilst T_r remains small, T_s determines the shift and T_r the width of the velocity distribution. This expression is found to be in good agreement with the results of numerical integration of the expression for the reaction rate coefficient (Draine & Katz 1986).

(ii) Each photoionization event is supposed to contribute an energy of 1 eV to the electron gas. A more accurate assessment of the rate of photoionization heating would suppose reliable knowledge of the flux of the ionizing radiation and of the frequency dependence of the ionization cross-sections.

(iii) Cooling of the neutral gas through collisional excitation of CO, OH and H_2O [see Flower, Pineau des Fôrets & Hartquist 1986 (Paper II)] is attributed thresholds of 5, 120 and 35 K. respectively. This change prevents the post-shock temperature falling to unrealistically low values, but is of no significance to the region of the shock.

(iv) In Papers I and II, only para-H_2 was included in the models. However, it is possible for ortho-H_2 to be the more abundant modification in the pre-shock gas, as ortho- and para-H_2 are believed to form, on grains, in the normal ratio of 3:1. Furthermore, ortho-H_2 may be produced, from para-H_2, through spin-changing collisions with H^0 in the hot gas of the precursor. Using the rate for this process ($8\times10^{-11}\exp(-3900/T_{\rm n})\,{\rm cm^3\,s^{-1}}$) from Schofield (1967), we have included ortho-para conversion in the MHD chemical model, starting from an assumed ortho:para ratio of 1:1.

(v) As noted in Paper II, the rate of radiative cooling by H_2, through rotational and vibrational transitions, is uncertain because of the inadequacy of the data pertaining to the rates of collisional excitation by H^0 and H_2. Further experimental or theoretical studies of these processes, for temperatures $T \approx 1000$ K, are urgently required. In the present study, we have used rates for the rotational excitation of H_2 ($0 \leqslant J \leqslant 6$) by He recently computed by Schaefer (1985, private communication), applying them without discrimination to excitation by both the He and H_2. The computed rate coefficients were found to be well fitted by a power-law dependence on temperature for $100 \leqslant T_{\rm n} \leqslant 600$ K, enabling extrapolation to higher temperatures to be made with reasonable confidence.

3 Results

3.1 HYDRODYNAMIC SHOCKS

In order to assess the importance of the magnetic field, it is first necessary to consider the properties of purely hydrodynamic models which incorporate the same chemical network. These one-fluid models are analogous to those computed by Elitzur & Watson (1980), the formation of CH^+ being driven by the thermal effect of the shock, rather than ambipolar diffusion which occurs in the MHD models considered below. However, the network of chemical reactions which we have included is much more extensive than the corresponding scheme of Elitzur & Watson (1980). Furthermore, several important rate coefficients, such as the rates of formation of CH^+ and photodissociation of OH, have been more reliably determined since 1980.

In Table 2(a), we present the computed column densities of relevant species, for a shock with velocity $u_s = 12\,\mathrm{km\,s^{-1}}$ and a range of atomic/molecular hydrogen density ratios. Analogous

Table 2. (a) Computed post-shock temperatures and column densities for hydrodynamic models with various molecular compositions of the pre-shock gas. The shock speed is $12\,\mathrm{km\,s^{-1}}$ and the radiative flux enhancement χ (flux of UV radiation incident on cloud/galactic background flux) is taken to be $\chi = 10$ in order that a direct comparison may be made with fig. 3 of Elitzur & Watson (1980). (b) As Table (a) for various shock velocities. The pre-shock densities are $n_1(H^0) = 16\,\mathrm{cm^{-3}}$ and $n_1(H_2) = 2\,\mathrm{cm^{-3}}$. The radiative flux enhancement χ is 1 [*cf.* figs 4 and 5 of Elitzur & Watson (1980)].

(a)

n_1 (H^0) (cm^{-3})	n_1 (H_2) (cm^{-3})	T_2 (K)	log N (cm^{-2}) CH^+	CH	OH	H_2 (J=4)	H_2 (J=6)
0.4	9.8	5181	12.00	12.48	13.08	16.40	15.29
2.	9.	5112	12.04	12.11	13.09	16.40	15.32
4.	8.	5022	12.15	11.85	13.11	16.41	15.35
8.	6.	4832	12.26	11.45	13.11	16.42	15.39
12.	4.	4627	12.30	11.04	13.11	16.42	15.42
16.	2.	4405	12.30	10.46	13.08	16.40	15.44
19.6	0.2	4188	12.18	9.11	12.91	16.19	15.30

(b)

u_s (km s^{-1})	T_2 (K)	log N (cm^{-2}) CH^+	CH	OH	H_2 (J=4)	H_2 (J=6)
10	3059	11.98	10.30	13.15	16.28	15.08
12	4405	12.28	10.85	13.38	16.41	15.43
14	5995	12.49	11.32	13.53	16.49	15.69
16	7831	12.65	11.66	13.63	16.56	15.89
18	9911	12.79	11.93	13.72	16.61	16.05

results for a pre-shock composition of $n(H^0)=16\,cm^{-3}$ and $n(H_2)=2\,cm^{-3}$, and a range of shock velocities, are given in Table 2(b). These calculations may be compared with the corresponding results of Elitzur & Watson (1980, figs 3–5).

Particularly noticeable in Table 2(a) is the constancy of the column density of H_2 in its excited rotational state $J=4$. This feature arises from the dominance of collisional excitation from $J=2$ to $J=4$, followed by radiative decay, in the cooling of these models. The rôle of molecular hydrogen cooling has been considered in the preceding Paper II.

The CH^+ column densities in Table 2(a) fall substantially below the observed values, which can exceed $10^{13}\,cm^{-2}$. In this respect, our conclusions, based upon an extended and updated chemical network, differ substantially from those of Elitzur & Watson (1980), but are confirmed by independent calculations of Mitchell & Watt (1985). The OH column densities are also rather lower than observed, for example in ζ Oph, o Per, and ζ Per (see Table 5 below), owing to the enhanced rôle of photodissociation reactions when $\chi=10$, but we recall that OH is also produced in the cold ambient medium (Black & Dalgarno 1977).

Somewhat larger column densities of CH^+ can be produced in models with higher shock speeds [Table 2(b)], although we note that our models tend to overestimate both the CH^+ and the OH abundance owing to the neglect of vibrational cooling. In any case, very high shock velocities ($u_s \approx 20\,km\,s^{-1}$) are required for the column density of CH^+ to approach $10^{13}\,cm^{-2}$. In models with a standard galactic background radiation field ($\chi=1$), the CH^+ column density is found to be strongly dependent on the fraction of molecular hydrogen present in the gas, increasing by almost an order of magnitude as this fraction, $n(H_2)/[n(H_2)+n(H^0)]$, decreases from 0.96 to 0.11. We shall return to this point in the discussion below.

The variation of the CH column density with the initial fraction of molecular hydrogen in the gas is similar to that found by Elitzur & Watson (1980). Our computed values of N(CH) tend to be less than observed, but CH is also produced in the ambient medium (Black & Dalgarno 1977).

3.2 MAGNETOHYDRODYNAMIC SHOCKS

It was shown in Paper I that the structure of a MHD shock is strongly dependent on the chemistry, particularly the ion–molecule chemistry. In Section 2, we have outlined the chemical scheme included in the present study, which is designed to reproduce the ionization structure of the shock and the interaction of the gas flow with the magnetic field. Our chemical scheme also predicts the abundances and column densities of 28 atomic and molecular species, some of which are preferentially formed in shocks. We shall consider the dependence of the predicted column densities of these species on the parameters defining the shock, in particular, the shock speed, the initial magnetic field strength and the molecular composition of the pre-shock gas.

3.2.1 Dependence on the shock speed, u_s

In Table 3, we have shown the dependence of the physical parameters within the shock on the shock speed, u_s. Also given are the computed column densities of CH^+, CH and OH and of the excited rotational states, $2 \leqslant J \leqslant 6$, of H_2. All of these species are produced in the region of the shock, as may be seen from Figs 1–9. Their column densities increase rapidly with the shock speed. The initial energy flux ($erg\,cm^{-2}\,s^{-1}$) in the shock, $\rho_0 u_s^3/2$, is radiated within the shock, the gas returning to its upstream temperature. Because the spontaneous radiative transition probability for the $J'=2 \rightarrow J''=0$ transition in H_2 is very small [$A(2\rightarrow 0)=2.94\times10^{-11}\,s^{-1}$,

Table 3. Computed physical parameters and column densities for MHD shocks with various shock velocities. $|u_i - u_n|_{max}$ is the maximum ion–neutral velocity difference (see Fig. 1) and T_n(max) is the maximum neutral temperature within the shock; l is the length of ion–neutral decoupling, see Figs 1–2. The initial magnetic induction B_0 is 5μG and the upstream densities are $n_0(H^0) = 0.4\,cm^{-3}$ and $n_0(H_2) = 9.8\,cm^{-3}$. The radiative flux enhancement is $\chi = 1$.

u_s (km s^{-1})	$\lvert u_i - u_n \rvert_{max}$ (km s^{-1})	T_n (max) (K)	l (10^{17} cm)	CH^+	CH	OH	H_2 (J) 2	3	4	5	6
8	3.1	762	1.2	12.04	13.26	12.08	17.49	16.70	15.32	13.65	11.46
10	4.6	925	1.4	12.93	13.92	12.76	17.68	17.10	15.85	14.40	12.36
12	6.2	1130	1.7	13.23	14.11	13.15	17.80	17.36	16.17	14.86	12.91
15	8.8	1330	1.9	13.48	14.28	13.52	17.93	17.61	16.43	15.32	13.45
17	10.5	1450	2.2	13.59	14.34	13.72	17.99	17.74	16.64	15.54	13.71
20	13.1	1600	2.4	13.71	14.40	13.96	18.06	17.90	16.82	15.80	14.01

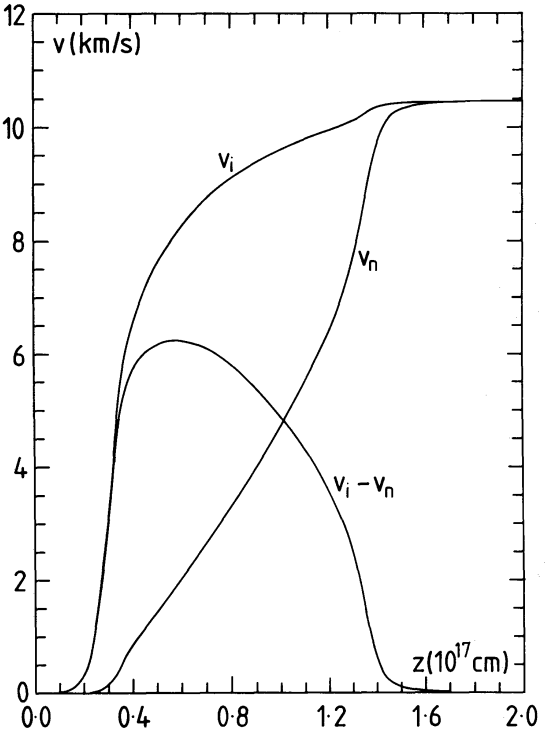

Figure 1. Velocity profiles of the reference model discussed in the text whose initial values are given in Table 6. The flow speeds, v, are expressed in an inertial frame, i.e. $v = u_s - u$, where u_s is the shock speed and u is the flow speed relative to the shock.

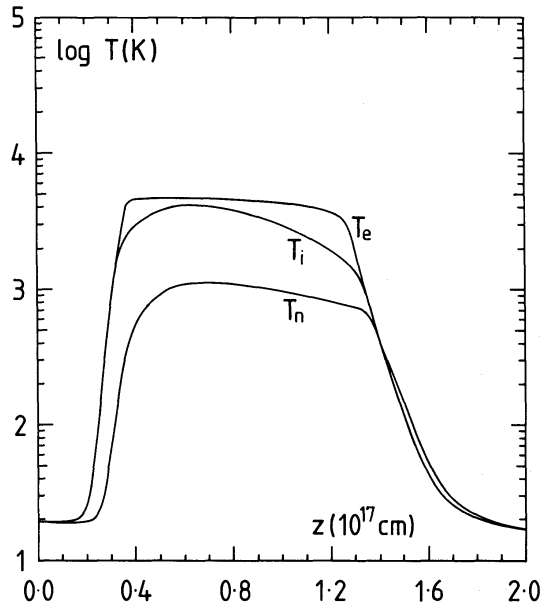

Figure 2. Neutral, ionic and electronic temperature profiles for the reference model.

Turner, Kirby-Docken & Dalgarno 1977], the populations of the $J' = 2$ and $J'' = 0$ rotational levels almost thermalize within the shock, even for the low upstream densities ($n_0 \approx 10\,\mathrm{cm}^{-3}$) which we are considering. The dominant cooling transition in H_2 is then $J' = 4 \rightarrow J'' = 2$, excitation of $J > 4$ requiring higher density and temperature.

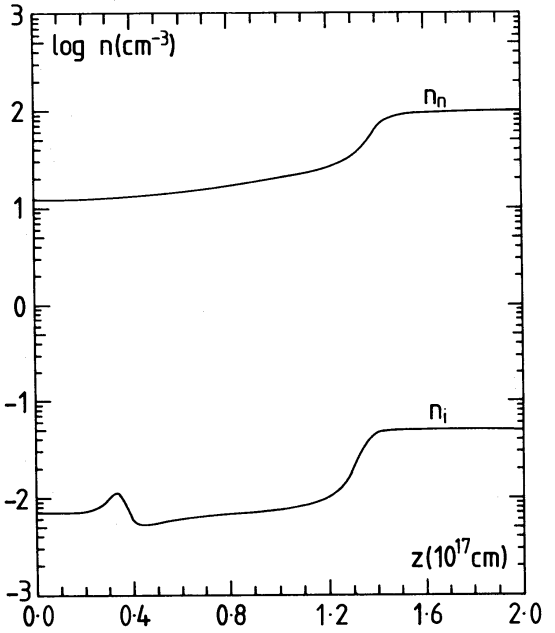

Figure 3. Neutral and ion density profiles for the reference model.

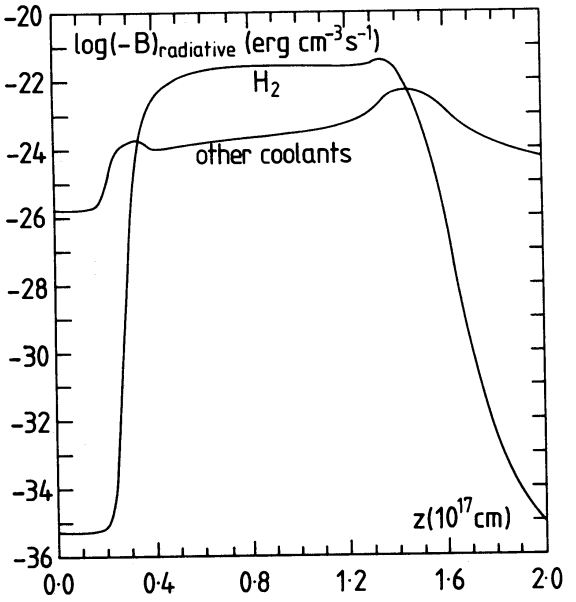

Figure 4. Rates of cooling in the reference model through collisional excitation of H_2 and through all other collisional processes.

If we assume that all of the shock energy is radiated in the $4\rightarrow 2$ transition, we have (*cf.* Paper II)

$$\varrho_0 u_s^3/2 = \int n(J=4)\, A(4\rightarrow 2)\, [E(4)-E(2)]\, dz$$
$$= N(J=4)\, A(4\rightarrow 2)\, [E(4)-E(2)]. \qquad (3.1)$$

Thus, at this level of approximation, we expect that $N(J=4) \propto u_s^3$. In fact, for the important range $8 \leqslant u_s \leqslant 20\,\mathrm{km\,s^{-1}}$, $N(J=4)$ increases even more rapidly with u_s, owing to the greater

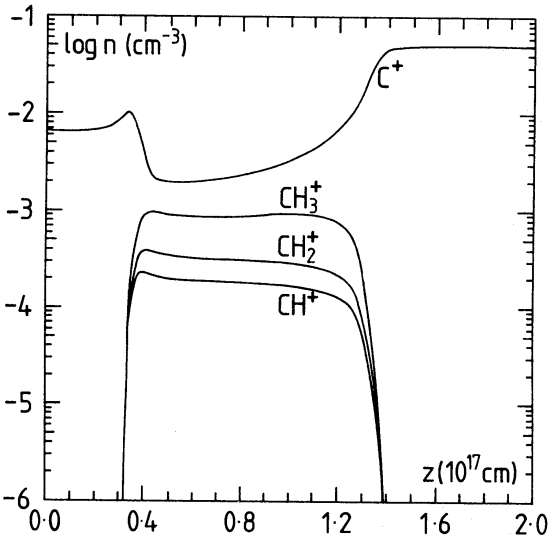

Figure 5. Variation of the abundances of the carbon-bearing ions for the reference model.

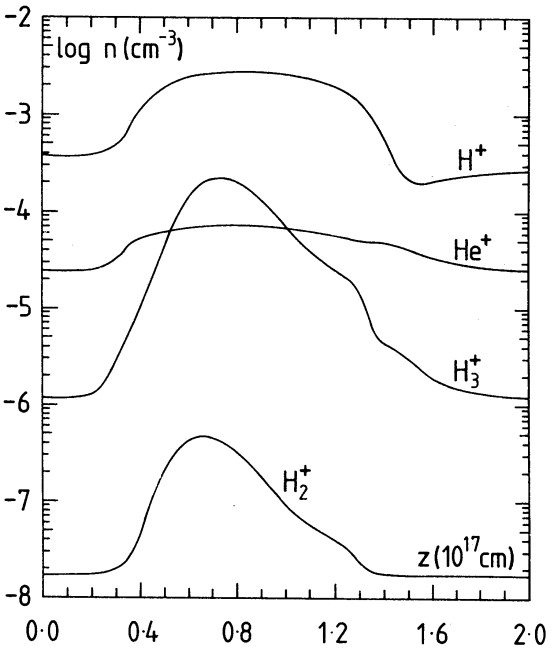

Figure 6. As Fig. 5 for hydrogen and helium ions.

relative importance of cooling by processes other than the rotational excitation of H_2 at the lower shock speeds, for which the maximum temperature within the shock is lower.

The column densities of CH^+ and OH also increase rapidly with the shock speed. It will be recalled that the reactions leading to the formation of these species, (1.1) and (1.2) above, are both endothermic, by 4640 and 2980 K, respectively. The reaction forming OH proceeds more rapidly as u_s increases, owing to the rise in the maximum temperature within the shock, $T_n(\max)$. The rate of formation of CH^+ is enhanced for the same reason, but, in this case, a more important factor is the increase in the maximum ion–neutral velocity difference, $|u_i - u_n|_{\max}$, enabling the reaction to be driven by ambipolar diffusion.

We see from Table 3 that column densities of CH^+ much in excess of $10^{13}\,cm^{-2}$ are readily attained in the shock, at the higher shock speeds. Indeed, the column densities predicted for

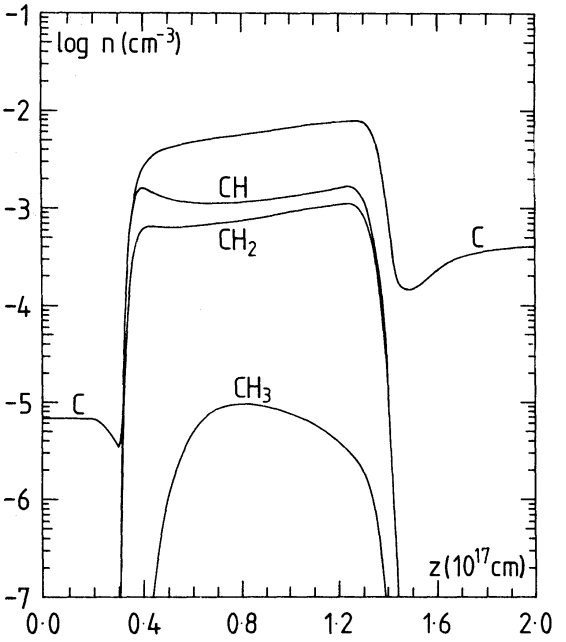

Figure 7. As Fig. 5 for the carbon-bearing neutrals.

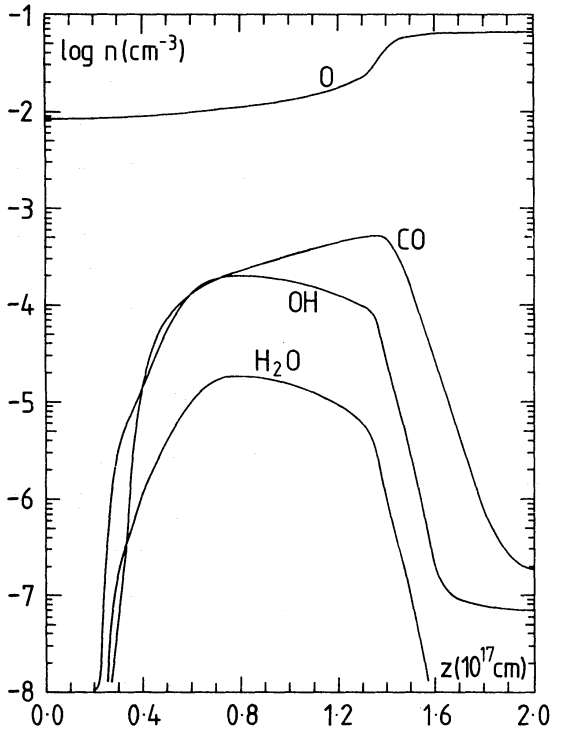

Figure 8. As Fig. 5 for oxygen-bearing neutrals.

$u_s \geqslant 16$ km s^{-1} are higher than observed (*cf.* Table 5). Such large shock velocities are incompatible with the velocity shifts of the CH^+ absorption lines which are probably observed (Crutcher 1979). We note that the interpretation of such velocity shifts in the context of MHD shocks is complicated by the existence of a precursor. The velocity difference between species, such as CH^+ and OH, produced within the precursor, depends on the variation of their densities and of the velocities of the ionized and neutral fluids. Similarly, the velocity differences between these

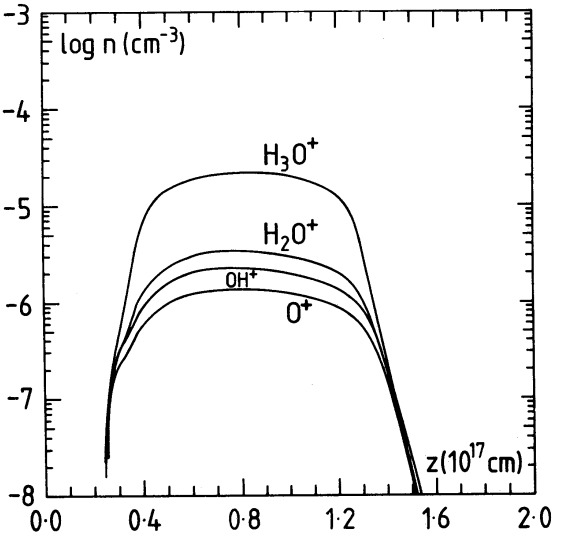

Figure 9. As Fig. 5 for oxygen-bearing ions.

species and the pre-shock gas depend on the variations of the appropriate fluid velocities, weighted by the molecular abundances, through the precursor.

3.2.2 *Dependence on the initial magnetic induction, B_0*

In contrast to the strong dependence of the computed column densities on the shock velocity, we see from Table 4 that the column densities are relatively insensitive to the initial magnetic induction, B_0. As B_0 increases, both $T_n(\max)$ and $|u_i - u_n|_{\max}$ decrease. For $B_0 \gtrsim 10\mu$G, $|u_i - u_n|_{\max}$ becomes insufficient for ambipolar diffusion to drive reaction (1.1). Thus, large magnetic field strengths are incompatible with the observed column densities of CH^+. This fact suggests the interesting possibility of determining an upper limit to the magnetic field strength in the medium from the observed column densities of species such as CH^+.

3.2.3 *Dependence on the fraction of molecular hydrogen in the gas*

Table 5 illustrates the variation of the physical parameters within the shock and of the computed column densities with the fraction of molecular hydrogen, $n(H_2)/[n(H_2)+n(H^0)]$. We see, once again, from this table the insensitivity of the column density of H_2 ($J=4$) to the molecular fraction. As noted above, this insensitivity derives from the relationship between $N(J=4)$ and the cooling of the shock. A reduction in the molecular fraction results in increases in $T_n(\max)$ and $N(OH)/N(CH^+)$.

The column density of CH^+ in Table 5 is seen to be insensitive to the molecular fraction of the gas. The principal reaction leading to the formation of CH^+ is (1.1) above, and the main destruction mechanism within the shock is

$$CH^+ + H_2 \rightarrow CH_2^+ + H + 700\,\text{K} \tag{3.2}$$

when $n(H_2)/n(H^0) \gtrsim 0.1$. Equating the rates of (1.1) and (3.2), we conclude that $n(CH^+) \propto n(C^+)$ in the region where ambipolar diffusion is sufficient to drive the $C^+(H_2, H)CH^+$ reaction. The width of this region is determined by the magnetohydrodynamical length-scale

$$L = \frac{(\mu_n + \mu_i)\, B_0^2}{\pi \varrho_{i0} \varrho_{n0} \langle \sigma v \rangle_{in} u_s}, \tag{3.3}$$

where ϱ_{i0} and ϱ_{n0} are the initial ion and neutral densities, μ denotes a mean molecular weight, and $\langle\sigma v\rangle_{in}$ the rate coefficient for ion–neutral elastic scattering. As C^+ is initially the principal heavy ion in the gas, $\varrho_{i0} \propto n(C^+)$ and hence $L \propto 1/n(C^+)$. We conclude that $N(CH^+) \propto N(C^+) L \approx$ constant. Clearly, this conclusion applies only to a two-fluid MHD shock and differs markedly from the results of the one-fluid, hydrodynamic calculations, discussed above.

3.2.4 Chemical abundances

As we have seen, the computed column densities of CH^+ are relatively independent of the upstream H/H_2 abundance ratio for shocks with $u_s \approx 10\,km\,s^{-1}$. Since the upstream H^+ abundance is dependent on this ratio, we may conclude that H^+-H_2 and H^+-H scattering cannot dominate the drag through a large, if any part of the precursor. Further, photodissociation rather than reactions with H must be the dominant mechanism breaking the larger neutral molecules and molecular ions into smaller species. Figs 1–9 present results for a reference model whose initial values are given in Table 6. In the reference model, we adopt a standard interstellar radiation field, $\chi = 1$.

We look first at the abundance of C^+ and H^+ in the reference model. The C^+ density initially rises due to compression and then falls as the $C^+(H_2, H)CH^+$ reaction removes it. Subsequently, compression begins to dominate again and the C^+ density rises. Note that the temperatures of all three fluids rise during the period before the C^+ density begins to decrease, subsequently level off and then drop slowly. The removal of C^+ acts as a thermostat: a rise in temperature leads to more rapid removal through the endothermic $C^+(H_2, H)CH^+$ reaction, but the consequent drop in the degree of ionization reduces the rate of heating through ambipolar diffusion. As discussed in Section 2, H^+ is removed on a longer scale. The peak H^+/C^+ abundance ratio approaches unity. Throughout the precursor the major source of C^+ is photoionization of atomic carbon. At neutral temperatures of the order of 1000 K, experienced in the precursor, the reaction $C(H_2, H)CH$, for which the rate coefficient has an exponential temperature dependence of $\exp(-14\,100/T_n)$, is slow relative to the photodissociation of CH and CH_2. In faster shocks with higher neutral temperatures, the CH_n abundances are enhanced considerably.

The most abundant molecular ion in the reference model is CH_3^+, which is only a few times less abundant than C^+ through much of the precursor. In contrast to the neutral species, C, the ions C^+, CH^+, and CH_2^+ react with molecular hydrogen to form bigger molecules at a rate which exceeds the photodissociation rate. Essentially, C^+ is converted to CH_3^+ by a sequence of comparatively fast hydrogen abstraction reactions and CH_3^+ then recombines, forming CH and CH_2, which are photodissociated to C, which is then photoionized.

The oxygen chemistry is also affected by the low neutral temperature. The reaction rate coefficient of $O(H_2, H)OH$ is about $6\times10^{-13}\,cm^3\,s^{-1}$ at the peak neutral temperature but the photodissociation of OH proceeds at a rate of $4\times10^{-10}\,s^{-1}$, resulting in O always being at least 50 times more abundant than OH. The reaction rate coefficient of $OH(H_2, H)H_2O$ is $4\times10^{-12}\,cm^3\,s^{-1}$ at the maximum neutral temperature. The photodissociation rate is approximately $6\times10^{-10}\,s^{-1}$ and, even at the peak neutral temperature, H_2O remains less abundant than OH in the reference model. The production of oxygen-bearing ions is dominated by the charge transfer of O with H^+:O^+ formation is followed by the hydrogen abstraction sequence, which is rapid, and OH_3^+ is the most abundant oxygen-bearing ion. Its recombination leads to the formation of OH and H_2O which, as noted above, are photodissociated quickly to form O.

In denser regions and in shocks in which the post-shock neutral temperature is higher, reactions of O and C with H_2 will be faster than the photodissociation reactions. When the neutral hydrogen

Table 4. As Table 3 for various values of the initial magnetic induction, B_0. The shock speed is 12 km s^{-1}.

B (μG)	$\lvert u_i-u_n\rvert_{max}$ (km s^{-1})	T_n (max) (K)	ℓ (10^{17} cm)	CH^+	CH	OH	H_2 (J) 2	3	4	5	6
5	6.2	1130	1.7	13.23	14.11	13.15	17.80	17.36	16.17	14.86	12.91
6	5.6	1040	1.9	13.20	14.11	13.08	17.81	17.33	16.11	14.76	12.77
8	4.5	900	2.3	13.08	14.04	12.89	17.83	17.24	15.96	14.49	12.42
10	3.6	780	3.0	12.86	13.89	12.65	17.86	17.12	15.76	14.15	11.98
12	2.7	680	4.1	12.23	13.38	12.28	17.87	16.95	15.47	13.68	11.37

Table 5. As Table 3 for various molecular compositions of the preshock gas. The initial magnetic induction B_0 is 5μG. Comparison is made with observations of ζ Per, o Per and ζ Oph. All the observed column densities of CH^+ are normalized to the oscillator strength recommended by Lambert & Danks (1985) ($f=5.5\times10^{-3}$) for the observed transition. The shock speeds are, respectively, 9, 11 and 16 km s^{-1} in Tables 5(a), (b) and (c).

n_o (H^o) (cm^{-3})	n_o (H_2) (cm^{-3})	$\lvert u_i-u_n\rvert_{max}$ (km s^{-1})	T_n (max) (K)	ℓ (10^{17} cm)	CH^+	CH	OH	H_2 (J) 2	3	4	5	6
0.4	9.8	3.84	840	1.3	12.65	13.72	12.49	17.60	16.93	15.63	14.08	11.97
2	9	3.84	841	1.2	12.59	13.43	12.43	17.51	16.89	15.64	14.24	12.27
4	8	3.83	854	1.1	12.53	13.11	12.36	17.40	16.85	15.65	14.37	12.51
8	6	3.83	900	1.0	12.40	12.57	12.23	17.20	16.77	15.63	14.55	12.80
				ζ Per	12.56	13.04 13.38	13.44 13.89	18.02 18.08	16.11 16.43	14.95 15.07	14.32 14.40	---
(a)				Reference	(1)	(2)	(3)	(3)	(3)	(3)	(3)	

n_o (H^o) (cm^{-3})	n_o (H_2) (cm^{-3})	$\|u_i-u_n\|_{max}$ (km s^{-1})	T_n (max) (K)	ℓ (10^{17} cm)	CH^+	CH	OH	H_2 (J) 2	3	4	5	6
0.4	9.8	5.4	1050	1.5	13.11	14.04	12.97	17.74	17.24	16.03	14.66	12.66
2	9	5.7	1062	1.3	13.08	13.75	12.96	17.61	17.22	16.03	14.84	12.94
4	8	5.7	1080	1.2	13.08	13.45	12.91	17.46	17.17	15.99	14.96	13.12
8	6	5.6	1150	1.0	13.00	12.92	12.81	17.20	17.04	15.91	15.09	13.35
				o Per	13.05	13.53	14.28 14.59	17.93 18.09	17.54 17.64	16.09 16.79	14.41 14.81	≤14.01
(b)				Reference	(4)	(4)	(5)	(5)	(5)	(5)	(5)	(5)

n_o (H^o) (cm^{-3})	n_o (H_2) (cm^{-3})	$\|u_i-u_n\|_{max}$ (km s^{-1})	T_n (max) (K)	ℓ (10^{17} cm)	CH^+	CH	OH	H_2 (J) 2	3	4	5	6
0.4	9.8	9.3	1400	2.1	13.54	14.30	13.61	17.96	17.68	16.57	15.43	13.59
2	9	9.6	1400	2.0	13.56	14.00	13.54	17.81	17.66	16.48	15.53	13.67
4	8	9.6	1420	1.7	13.57	13.71	13.48	17.65	17.59	16.41	15.60	13.77
8	6	9.5	1500	1.3	13.51	13.15	13.36	17.35	17.40	16.29	15.66	13.93
				ζ Oph	13.53	13.53	13.71	18.56	17.07	15.68	14.77	13.58
(c)				Reference	(8)	(6)	(7)	(6)	(6)	(6)	(6)	(6)

References:

(1) Hobbs (1973)
(2) Chaffee & Lutz (1977)
(3) Snow (1977)
(4) Chaffee (1974)
(5) Snow (1976)
(6) Morton (1975)
(7) Black & Dalgarno (1977)
(8) Lambert & Danks (1985)

Table 6. Initial values of the standard model appearing in Figs 1–9. Numbers in brackets are powers of 10. These values are deduced from the equilibrium state including H_2 formation on dust grains [H+(H+grain)→H_2+grain] with a rate of $3\times10^{-17}n(H^0)\,s^{-1}$ (Hollenbach, Werner & Salpeter 1971). The initial ortho-H_2:para-H_2 ratio is taken to be 1:1 in this and all other models.

Parameter	Initial value	Unit
$n(H_2)$	9.8	cm^{-3}
$n(H^0)$	0.4	cm^{-3}
$T_e=T_i=T_n$	20	K
u_s	12	$km\,s^{-1}$
B_0	5	μG
$n(He)$	2.0	cm^{-3}
$n(O)$	8.5 (−3)	cm^{-3}
$n(H^+)$	3.75 (−4)	cm^{-3}
$n(He^+)$	2.43 (−5)	cm^{-3}
$n(C^+)$	6.60 (−3)	cm^{-3}

abstraction reactions dominate, the CH^+ column density will depend on the upstream abundance ratio H/H_2.

3.2.5 Comparison with observations

In Table 5, we compare the computed column densities of species which are formed in the precursors of MHD shocks with observations of ζ Oph, *o* Per and ζ Per. Acceptable column densities of CH^+ can readily be produced in MHD shock models with modest speeds ($9\leqslant u_s\leqslant16\,km\,s^{-1}$) and initial magnetic induction ($B_0=5\mu G$). The values of $N(OH)$ and $N(CH)$ in these same models are lower limits to the true values, as OH and CH are also produced in the ambient medium (Black & Dalgarno 1977). Furthermore, owing to its sensitivity to the initial fraction of molecular hydrogen in the gas, $N(CH)$ may be more readily fitted to the observations.

In the case of *o* Per [Table 5(b)], the column density of CH predicted by the shock models is smaller than the observed column density, as required, for $n_0(H_2)/n_0(H^0)\leqslant2$, when a good fit is also obtained to $N(CH^+)$. The computed column densities of the excited rotational states of H_2, $2\leqslant J\leqslant6$, are then somewhat lower than observed for $2\leqslant J\leqslant4$, but marginally higher than observed for $J=5$. However, it should be borne in mind that radiative (ultraviolet) pumping may also be expected to contribute to $N[H_2(J)]$, and so the computed excited state column densities are lower limits to the true values.

In the cases of ζ Per and ζ Oph [Table 5(a) and (c), respectively], good fits to the observed CH^+ column densities and acceptable lower limits to $N(CH)$ are again obtained for $n_0(H_2)/n_0(H^0)\leqslant2$. However, in this case, the computed $H_2(J)$ column densities are substantially *higher* than observed for $J=3$, 4, and (in the case of ζ Oph) 5. By reducing the shock speed, and hence the initial flux of energy in the models, the computed values of $N[H_2(J)]$ could be reduced, but such action would have the undesirable effect of also reducing $N(CH^+)$ below the observed values.

4 Conclusions

We have studied the formation of CH^+ in a range of models of shocks propagating in diffuse molecular clouds. A chemical network of over 150 reactions was designed to reproduce the

ionization structure of the shock and the pathways leading to the formation and destruction of molecules such as CH^+ and OH. Our main conclusions are:

(i) that the abundance of CH^+ predicted by one-fluid hydrodynamic shock models is unacceptably low compared with observations of diffuse interstellar clouds;

(ii) that column densities of CH^+ in agreement with observations of the clouds along the lines-of-sight to ζ Oph, o Per and ζ Per are readily produced in MHD models with magnetic precursors.

However, the computed values of $N[H_2(J)]$, $J=3$ and $J=4$, are larger than observed in ζ Per and ζ Oph. The latter discrepancy indicates that the initial flux of energy in these shock models may be overestimated. In turn, this would imply that the computed CH^+ column densities are overestimated, jeopardizing the apparent agreement with the observed values of $N(CH^+)$. At this stage, we believe that it would be premature to assert that CH^+ is produced universally in interstellar shocks in quantities sufficient to satisfy all observational constraints, although MHD shock production may be the dominant mechanism along certain lines-of-sight, e.g. to o Per. Detailed modelling of individual lines-of-sight, including a component of shocked gas, is now required.

Finally, we note that our conclusions might be modified if it transpires that key dissociative recombination reactions, particularly reactions 21–26 inclusive, are substantially overestimated. The work of Smith & Adams (1984) on the dissociative recombination of H_3^+ shows that the rates of such processes can be strongly dependent on the initial vibrational state distribution which may be very different in interstellar shocks and laboratory plasmas.

Acknowledgments

This work has been supported by the NATO research grant no. 085/84. AD acknowledges support from the Astronomy Section of the National Science Foundation. The award of a SERC Visiting Fellowship to TWH is also acknowledged. The calculations were largely carried out at the Centre Inter-Régional de Calcul Electronique (Orsay).

References

Aannestad, P., 1973. *Astrophys. J.*, **186,** L29.
Adams, N. G., Smith, D. & Millar, T. J., 1984. *Mon. Not. R. astr. Soc.*, **211,** 857.
Black, J. H. & Dalgarno, A., 1977. *Astrophys. J. Suppl.*, **34,** 405.
Chaffee, F. H., 1974. *Astrophys. J.*, **189,** 427.
Chaffee, F. H. & Lutz, B. L., 1977. *Astrophys. J.*, **213,** 394.
Chambaud, G., Launay, J. M., Levy, B., Millie, P., Roueff, E. & Tran Minh, F., 1980. *J. Phys. B: Atom. Molec. Phys.*, **13,** 4205.
Chesnavich, W. J., Akin, V. E. & Webb, D. A., 1984. *Astrophys. J.*, **287,** 676.
Cohen, N. & Westburg, K. R., 1983. *J. Phys. Chem. Ref. Data,* **12,** 531.
Crutcher, R. M., 1979. *Astrophys. J.*, **231,** L151.
Dalgarno, A., 1952. *Proc. Phys. Soc. Lond. A,* **65,** 66.
Dalgarno, A., 1976. In: *Atomic Processes and Applications,* p. 109, eds Burke, P. G. & Moiseiwitsch, B. L., North-Holland, Amsterdam.
Dalgarno, A. 1986. *Q. Jl. R. astr. Soc.*, **27,** 83.
Draine, B. T., 1980. *Astrophys. J.*, **241,** 1021.
Draine, B. T. & Katz, N. S., 1986. *Astrophys. J.*, submitted.
Elitzur, M. & Watson, W. D., 1978. *Astrophys. J.*, **222,** L141.
Elitzur, M. & Watson, W. D., 1980. *Astrophys. J.*, **236,** 172.
Ervin, K. M. & Armentrout, P. B., 1984. *J. chem. Phys.*, **80,** 2978.

Federer, W., Villinger, H., Howorka, F., Lindinger, W., Tosi, P., Basi, D. & Ferguson, E., 1984. *Phys. Rev. Lett.*, **52,** 2084.
Flower, D. R., Pineau des Forêts, G. & Hartquist, T. W., 1985. *Mon. Not. R. astr. Soc.*, **216,** 775 (Paper I).
Flower, D. R., Pineau des Forêts, G. & Hartquist, T. W., 1986. *Mon. Not. R. astr. Soc.*, **218,** 729 (Paper II).
Giusti-Suzor, A., Bardsley, J. N. & Derkits, C., 1983. *Phys. Rev. A,* **28,** 682.
Herbst, E., 1985. *Astr. Astrophys.*, **153,** 151.
Hobbs, L. M., 1973. *Astrophys. J.,* **181,** 79.
Hollenbach, D. J., Werner, M. & Salpeter, E. E., 1971. *Astrophys. J.,* **163,** 165.
Kim, J. L., Theard, L. P. & Huntress, W. T., 1975. *J. chem. Phys.*, **62,** 45.
Lambert, D. L. & Danks, A. C., 1985. *Astrophys. J.,* in press.
Lias, S. G., Liebman, J. F. & Levin, R. D., 1984. *J. Phys. Chem. Ref. Data,* **13,** 695.
Mitchell, G. F., 1984. *Astrophys. J. Suppl.,* **54,** 81.
Mitchell, G. F. & Deveau, T. J., 1983. *Astrophys. J.,* **266,** 646.
Mitchell, G. F. & Watt, G. D., 1985. *Astr. Astrophys.*, **151,** 121.
Mitchell, J. B. A. & McGowan, J. W., 1983. In: *The Physics of Ion–Ion and Electron–Ion Collisions,* p. 279, eds Brouillard, F. & McGowan, J. W., Plenum, New York.
Morton, D. C., 1975. *Astrophys. J.,* **197,** 85.
Mul, P. M., Mitchell, J. B. A., D'Angelo, V. S., De France, P., McGowan, J. Wm & Froelich, H., 1981. *J. Phys. B: Atom Molec. Phys.,* **14,** 1353.
Mullan, D. J., 1971. *Mon. Not. R. astr. Soc.,* **153,** 145.
Prasad, S. S. & Huntress, W. T., 1980. *Astrophys. J. Suppl.,* **43,** 1.
Roberge, W. G., Dalgarno, A. & Flannery, B. P., 1981. *Astrophys. J.,* **243,** 817.
Rosenstock, H. M., Draxl, K., Steiner, B. W. & Herron, J. T., 1977. *J. Phys. Chem. Ref. Data,* **6,** Suppl. 1.
Schofield, K., 1967. *Planet. Space Sci.,* **15,** 643.
Smith, D. & Adams, N. G., 1977. *Int. J. Mass. Spectrom. Ion Phys.,* **23,** 123.
Smith, D. & Adams, N. G., 1984. *Astrophys. J.,* **284,** L13.
Snow, T. P., 1976. *Astrophys. J.,* **204,** 759.
Snow, T. P., 1977. *Astrophys. J.,* **216,** 724.
Turner, J., Kirby-Docken, K. & Dalgarno, A., 1977. *Astrophys. J. Suppl.,* **35,** 281.
van Dishoeck, E. F. & Dalgarno, A., 1984. *Astrophys. J.,* **277,** 576.
Yung, Y. L. & Allen, M., 1983. Private communication, cited in Mitchell, G. F., 1984. *Astrophys. J. Suppl.,* **54,** 81.